Journal of Superconductivity: Incorporating Novel Magnetism, Vol. 16, No. 3, June 2003 (© 2003)

Magnetic Phase Diagram of $Ca_{1-x}Mn_xO$

S. Kolesnik[1] and B. Dabrowski[1]

Received and accepted 10 November 2002

Alternating current susceptibility and direct current magnetization have been studied for polycrystalline $Ca_{1-x}Mn_xO$. On increasing the Mn content, magnetic ordering changes from spin glass behavior for $0.25 \leq x \leq 0.4$ to antiferromagnetic order. The paramagnetic/antiferromagnetic transition is of second order for $0.5 \leq x \leq 0.65$ and of first order for $x \geq 0.7$. For low Mn concentrations, the high-temperature alternating current susceptibility can be described by a diluted Heisenberg magnet model developed for diluted magnetic semiconductors.

KEY WORDS: diluted magnetic semiconductor; $Ca_{1-x}Mn_xO$; spin glass behavior; antiferromagnetism.

Theoretical predictions of room temperature ferromagnetism in Mn-containing diluted magnetic semiconductors [1] recently brought wide attention to this class of materials. According to these calculations, *p*-type $Zn_{1-x}Mn_xO$ is a promising candidate for a room temperature ferromagnet. Pulsed-laser deposited $Zn_{1-x}Mn_xO$ thin films without intentional carrier doping show spin glass behavior [2]. According to this latter study, Mn can be dissolved in the ZnO matrix to over 35%. We have shown in a previous paper that the solubility of Mn in the zinc-blende structure of ZnO is less than 15% for polycrystalline samples under various oxygen pressure conditions. Samples obtained in air or argon are paramagnetic, while the high-pressure oxygen annealing induces spin glass–like behavior by precipitation of $ZnMnO_3$ in the paramagnetic matrix [3].

In this study we investigate polycrystalline $Ca_{1-x}Mn_xO$ ($x = 0.125$–1). Both end-member compounds, CaO and MnO, adopt the rock-salt structure and the complete range of solid solution can be achieved. This makes it possible to study a continuous evolution of magnetic properties from diamagnetic insulating/semiconducting CaO (energy gap $E_g = 7.09$ eV) [4] to antiferromagnetic insulating MnO ($T_N \simeq 120$ K, $E_g = 4$ eV), whose antiferromagnetic properties were already observed 70 years ago [5]. Because of similarity of the ionic radii (0.8 Å for Mn^{2+} and 0.99 Å for Ca^{2+}) Mn^{2+} ions should occupy a substitutional site in CaO in contrast to BaO (ionic radius of Ba^{2+} is equal to 1.34 Å), where Mn^{2+} ions locate off-center [6]. The CaO-MnO solid solution has been shown to form in the H_2He atmosphere above 1173K from carbonate precursors [23]. Thermodynamic functions of mixing have been determined at high temperatures for $Ca_{1-x}Mn_xO$ [7]. To our knowledge, the magnetic properties of this solid solution have not yet been reported. MnO undergoes a first-order transition to the antiferromagnetic state at $T_N = 115$–120 K [8,9]. This transition is accompanied by a trigonal deformation [10] to a slightly rhombohedral structure, compressed along the [111] direction [11]. The antiferromagnetic order, determined by neutron diffraction, is of type-II (AFII) in the fcc lattice and consists of (111) sheets of ferromagnetically ordered Mn^{2+} ions, which are antiferromagnetically coupled to the neighboring sheets along the [111] direction [12]. Magnetic properties of MnO have been explained in terms of two superexchange constants $J_1 = 10$ K and $J_2 = 11$ K for the nearest-neighbor (NN) and next-nearest-neighbor (NNN) interactions, respectively [13]. Recent local-density approximation (LDA) calculations [14] suggest relatively stronger NNN interactions, $J_1 = 9.8$ K and $J_2 = 24.5$ K. The small uniaxial stress along the [111] axis of the MnO crystal results in the clearly first-order transition and the increasing T_N [11]. This result has been ascribed

[1]Department of Physics, Northern Illinois University, DeKalb, Illinois 60115.

0896-1107/03/0600-0501/0

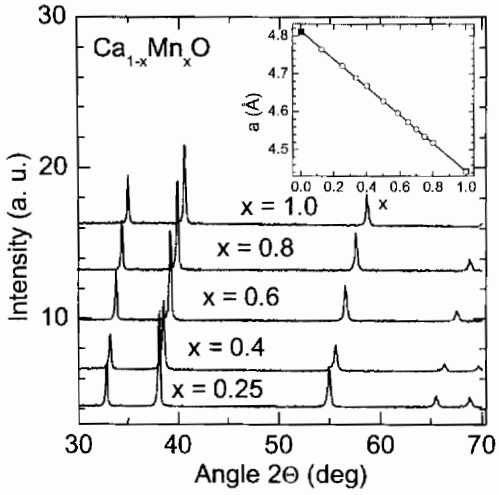

Fig. 1. X-ray diffraction patterns for several $Ca_{1-x}Mn_xO$ samples. Inset: lattice parameter, a, of the rock-salt structure of $Ca_{1-x}Mn_xO$. The solid line is a linear fit to the data. Solid squares are literature values for CaO and MnO.

to the strain-related suppression of T domains (which correspond to antiferromagnetic stacking along the four [111] directions within the crystal). Because of the presence of these T domains the first-order character of the antiferromagnetic/paramagnetic transition may be obscured. Recent heat capacity studies showed a continuous magnetic transition in small, stress-free, MnO crystals [15]. The application of large [111] stress ($1.2 < \tau \leq 5.5$ kbar) leads to a continuous transition, again [16]. Solid solution $Mn_{1-x}Ni_xO$ shows a linear increase of T_N upon increasing Ni concentration with preservation of the AFII structure [17]. Both end members of this series, MnO and NiO ($T_N \simeq 525$ K) show the same type of rhombohedral crystallographic distortions [12].

The mixture of $CaCO_3$ and MnO_2 was calcined in air several times at $T = 900$, 1000, 1100 C with intermediate grindings. The final synthesis stage was performed in a hydrogen atmosphere at $T =$ 1050 C. The alternating current (ac) susceptibility and direct current (dc) magnetization were measured using a Physical Property Measurement System (Quantum Design). The ac susceptibility was measured in the range 2.5–395 K, in the excitation field $H_{ac} = 14$ Oe at the frequency $\omega = 1$ kHz. The "zero-field–cooled" (M_{ZFC}) and "field-cooled" (M_{FC}) magnetizations were measured in a magnetic field of 1 kOe. M_{ZFC} was measured on warming after cooling in a zero magnetic field and switching the magnetic field on at $T = 5$ K. M_{FC} was subsequently measured on cooling in the magnetic field.

X-ray diffraction spectra have been collected using a Rigaku X-ray diffractometer. The sharp X-ray diffraction patterns, presented in Fig. 1 for several samples, indicate good quality, homogeneous material. The single-phase rock-salt-type structure is revealed for all the $Ca_{1-x}Mn_xO$ samples. Inset to Fig. 1 shows the lattice parameter, a, determined from the X-ray diffraction patterns using the GSAS refinement software. The lattice parameter, a, is linearly dependent on the Mn content x with a very good accuracy. The linear fit to the experimental data gives a dependence $a(x) = 4.812(1) - 0.369(2)x$ (Å). For CaO, the extrapolated a is equal to 4.812(1) Å, which is in agreement with the literature value $a = 4.81$ Å [18]. For our MnO sample, $a = 4.443(3)$ Å is very close to the literature value $a = 4.442$–4.446 Å [19]. A very good agreement between the measured lattice parameters and the linear dependence for all Mn concentrations suggests that the actual compositions and the nominal ones are the same.

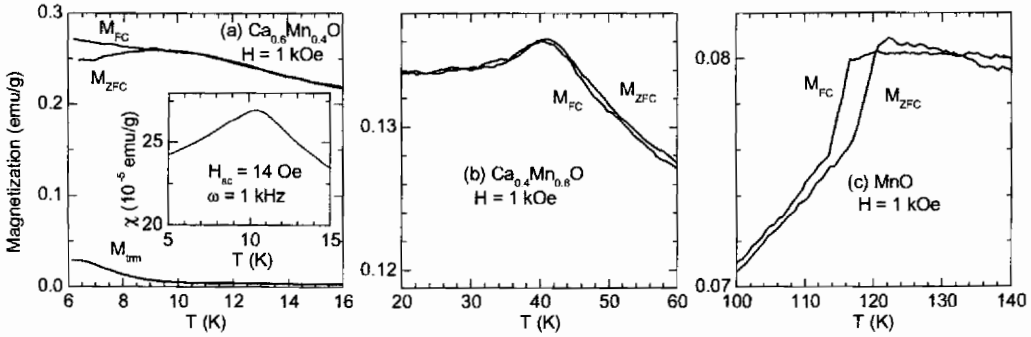

Fig. 2. "Zero-field–cooled" (M_{ZFC}), "field-cooled" (M_{FC}), and thermoremanent (M_{trm}) magnetizations for several $Ca_{1-x}Mn_xO$ samples. The inset shows the cusp in ac susceptibility. No thermoremanent magnetization was observed for $Ca_{0.4}Mn_{0.6}O$ or MnO.

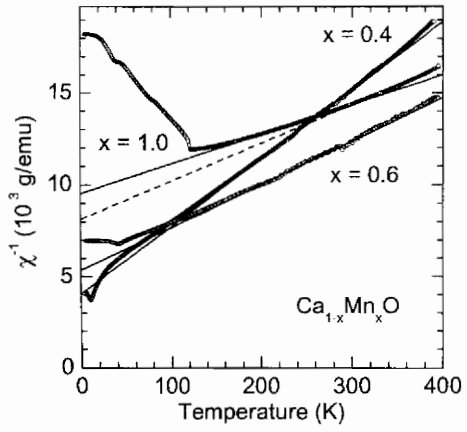

Fig. 4. Inverse ac susceptibility for $Ca_{1-x}Mn_xO$ samples. The solid lines are linear fits to the data in the range 200–300 K. The dashed line is a linear fit for $x = 1$ (i.e. MnO) in the range 300–390 K.

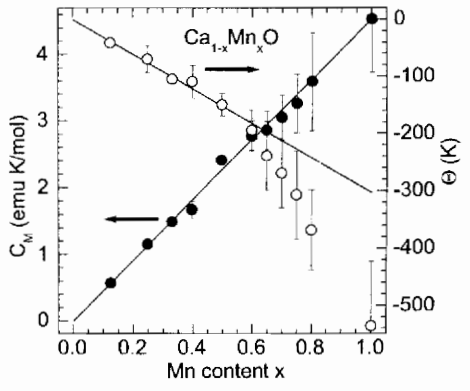

Fig. 5. Molar Curie constant $C_M(x)$ (solid circles) and Curie-Weiss temperatures $\Theta(x)$ (open circles) for $Ca_{1-x}Mn_xO$ samples. The solid lines are linear fits to the first three data points.

to the exchange integral between the nearest Mn neighbors J_1,

$$\frac{2J_1}{k_B} = \frac{3\Theta_0}{zS(S+1)}, \tag{4}$$

where $z = 12$ is the number of nearest neighbors in the rock-salt structure of $Ca_{1-x}Mn_xO$.

The inverse ac susceptibility for several $Ca_{1-x}Mn_xO$ samples is shown in Fig. 4. For low Mn concentrations, $x \leq 0.333$, the inverse ac susceptibility is linear with temperature in a wide range $T = 50$–390 K. Deviations from linearity (characteristic to diluted antiferromagnets and related to the interactions between next nearest neighboring Mn^{2+} ions [22]) are observed at lower temperatures. For higher Mn concentrations, the slope of the inverse susceptibility changes with temperature. We have analyzed the linear fits to the $\chi^{-1}(T)$ data in three temperature ranges: 100–200 K, 200–300 K, and 300–390 K.

The data points in Fig. 5 represent the parameters determined from the fit of Eq. (1) to the inverse susceptibility data in the temperature range 200–300 K. The values determined from the fits in the other two temperature regions are plotted as error bars. For a given x, the fit in the lower temperature range (100–200 K) gives higher absolute $\Theta(x)$ and larger $C_M(x)$ than the fit in the higher temperature range (300–390 K).

For diluted Heisenberg antiferromagnets it is expected that the material parameters $C_M(x)$ and $\Theta(x)$ are proportional to x. We have made linear fits to the first three data points (i.e., $0.125 \leq x \leq 0.333$, assuming that $C_M(x = 0) = 0$ and $\Theta(x = 0) = 0$). From these fits, we have obtained the extrapolated values $C_M(x = 1) = 4.53(4)$ emu K/mol and $\Theta_0 = -303(11)$ K. The value of C_M is close to those determined for Mn-containing II–VI diluted magnetic semiconductors [22]. From Eq. (2), calculated $S = 2.55(5)$, which is in perfect agreement with the effective spin of Mn^{2+} ion $S = 5/2$. The extrapolated Θ_0 is lower (in the sense of the absolute value) than the values found for diluted magnetic semiconductors ($\Theta_0 = -470$ to -831 K) [22]. We observe significant deviations from the linear behavior of $\Theta(x)$ for $x \geq 0.5$, where the antiferromagnetic order can be observed and the diluted magnet model is no longer valid. It is worth noting that for higher Mn concentrations the Curie-Weiss temperatures become comparable to or higher than our experimental temperature range, which increases the error of the determined values. However, we suggest that these deviations of $\Theta(x)$ from the linear behavior can be explained by the increasing contribution of NNN interactions between highly concentrated Mn^{2+} ions.

By including the NNN interactions we obtain the following modification of Eq. (3)

$$z\frac{2J_1}{k_B} + z_2\frac{2J_2}{k_B} = \frac{3\Theta(x)}{S(S+1)}, \tag{5}$$

where $z_2 = 6$ is the number of next-nearest neighbors. For MnO, for example, $\Theta = -536$ K. By using $2J_1/k_B = -8.7(3)$ K calculated from the extrapolated $\Theta_0 = -303$ K according to Eq. (4), we obtain $2J_2/k_B \approx -13.2$ K for MnO, which gives us a qualitative agreement with the LDA calculations [14], namely $J_2 > J_1$. However, the actual values of our exchange constants are significantly smaller than those

found in the literature (see references in Ref. [14]). Note that M. E. Lines and E. D. Jones [13] used an analogical formula to our Eq. (5) but without the factor 2. From their $\Theta = -540$ K, this gave as a result $(2J_2 + J_1)/k_B = 30.9$ K, which is twice as higher as our value.

In summary, we have determined the magnetic phase diagram of Mn-doped polycrystalline CaO samples. On increasing the Mn content, magnetic ordering changes from the spin glass behavior for $0.25 \leq x \leq 0.4$ to the antiferromagnetic order. The paramagnetic/antiferromagnetic transition is second order for $0.5 \leq x \leq 0.65$ and first order for $x \geq 0.7$. For low Mn contents, the ac susceptibility can be described by a diluted Heisenberg magnet model developed for diluted magnetic semiconductors.

ACKNOWLEDGMENTS

This work was supported by the DARPA/ONR and the State of Illinois under HECA.

REFERENCES

1. T. Dietl, H. Ohno, F. Matsukura, J. Cibert, and D. Ferrand, *Science* **287,** 1019 (2000).
2. T. Fukumura, Z. Jin, M. Kawasaki, T. Shono, T. Hasegawa, S. Koshihara, and H. Koinuma, *Appl. Phys. Lett.* **78,** 958 (2001).
3. S. Kolesnik, B. Dabrowski, and J. Mais, *J. Supercond: Incorp. Novel Magnetism* **15,** 251 (2002).
4. R. C. Whited and W. C. Walker, *Phys. Rev.* **188,** 1380 (1969).
5. R. W. Tyler, *Phys. Rev.* **44,** 776 (1933).
6. J. A. van Winsum, T. Lee, and H. W. den Hartog, *Phys. Rev. B* **18,** 173 (1978).
7. G. Róg, A. Kozlowska-Róg, W. Pycior, and K. Zakuła, *J. Solid State Chem.* **100,** 115 (1992).
8. D. Seino, S. Miyahara, and Y. Noro, *Phys. Lett. A* **44,** 35 (1973).
9. G. Srinivasan and M. S. Seehra, *Phys. Rev. B* **28,** 6542 (1983).
10. B. Morosin, *Phys. Rev. B* **1,** 236 (1970).
11. D. Bloch and R. Maury, *Phys. Rev. B* **7,** 4883 (1973).
12. C. G. Shull, W. A. Strausser, and E. O. Wollan, *Phys. Rev.* **83,** 333 (1951); W. L. Roth, *Phys. Rev.* **110,** 1333 (1958).
13. M. E. Lines and E. D. Jones, *Phys. Rev.* **139,** A1313 (1965).
14. J. E. Pask, D. J. Singh, I. I. Mazin, C. S. Hellberg, and J. Kortus, *Phys. Rev. B* **64,** 024403 (2001).
15. B. F. Woodfield, J. L. Shapiro, R. Stevens, J. Boerio-Goates, and M. L. Wilson, *Phys. Rev. B* **60,** 7335 (1999).
16. D. Bloch, D. Hermann-Ronzaud, C. Vettier, W. B. Yelon, and R. Alben, *Phys. Rev. Lett.* **35,** 963 (1975).
17. A. K. Cheetham and D. A. O. Hope, *Phys. Rev. B* **27,** 6964 (1983).
18. H. F. McMurdie, M. C. Morris, E. H. Evans, B. Paretzkin, W. Wong-Ng, and C. R. Hubbard, *Powder Diffract.* **1,** 265 (1986); B. Reardon and C. Hubbard, TM-11948, Oak Ridge Natl. Lab. Rep. (ORNL) (U.S.), 1992.
19. C. A. Barrett and E. B. Evans, *J. Am. Ceram. Soc.* **47,** 533 (1964); S. Sasaki, K. Fujino, T. Takeuchi, and R. Sadanaga, *Acta Crystallogr., Sect. A* **36,** 904 (1980).
20. A. Twardowski, H. J. M. Swagten, W. J. M. de Jonge, and M. Demianiuk, *Phys. Rev. B* **36,** 7013 (1987).
21. C. J. M. Denissen, S. Dakun, K. Kopinga, W. J. M. de Jonge, H. Nishihara, T. Sakakibara, and T. Goto, *Phys. Rev. B* **36,** 5316 (1987); R. R. Gałązka, S. Nagata, and P. H. Keesom, *Phys. Rev. B* **22,** 3344 (1980).
22. J. Spałek, A. Lewicki, Z. Tarnawski, J. K. Furdyna, R. R. Gałązka, and Z. Obuszko, *Phys. Rev. B* **33,** 3407 (1986).
23. K. R. Poeppelmeier, H. S. Horowitz, and J. M. Longo, *J. Less-Common Metals* **116,** 219 (1986).

Three different kinds of magnetic transitions observed for $Ca_{1-x}Mn_xO$ are illustrated in Fig. 2. For $x = 0.25$–0.4, the spin glass behavior is observed at low temperatures. A difference between the "zero-field–cooled" (M_{ZFC}) and "field-cooled" (M_{FC}) magnetizations, which is characteristic of spin glass behavior, is shown in Fig. 2a for $x = 0.4$. The presence of the thermoremanent (M_{trm}) magnetization at low temperatures supports this observation. The inset to Fig. 2a shows a cusp in the ac susceptibility. The temperature, at which the cusp is maximum defines the spin glass freezing temperature, T_f. Similar cusp was observed for the $x = 0.333$ sample and a kink on the ac susceptibility for $x = 0.25$. The same type of spin glass behavior has been previously observed for Mn-containing diluted magnetic semiconductors (e.g. $Zn_{1-x}Mn_xSe$ [20] and $Cd_{1-x}Mn_x$ Te [21]), where a cusp was observed for high Mn concentrations and a kink for low Mn concentrations.

For $x = 0.5$–0.65, M_{ZFC} and M_{FC} curves trace each other and no thermoremanent magnetization is observed. This behavior, presented in Fig. 2(b) indicates a continuous (second-order) paramagnetic/antiferromagnetic transition. For higher Mn concentrations, $x \geq 0.7$ including MnO, the paramagnetic/antiferromagnetic transition is accompanied by a hysteresis, clearly observed both in the ac susceptibility and dc magnetization (see Fig. 2c). This hysteresis is a sign of the discontinuous first-order transition.

The observed magnetic transition temperatures are collected in Fig. 3. The $x = 0.125$ sample is paramagnetic down to $T = 2.5$ K. The $x = 0.25$–0.4 samples show spin glass behavior at increasing temperatures with increasing Mn content. The antiferromagnetic transition temperatures for $x \geq 0.5$ are defined as the temperatures for which the temperature dependence of the ac susceptibility has the maximum slope, i.e., slightly below the observed maximum of $\chi(T)$. For the first-order transitions, ($x \geq 0.7$), we used the transition temperatures, which were determined on warming (M_{ZFC}). The transition temperatures in all the Mn-concentration regions seem to continuously change with x, but no common scaling has been determined. The spin glass behavior at low Mn concentrations is quantitatively similar to the behavior of wurtzite and zinc-blende diluted magnetic semiconductors. The temperature dependence of the ac susceptibility for $x \geq 0.5$ is almost identical with that of the dc magnetization. The width of the thermal hysteresis ΔT in the ac susceptibility at the antiferromagnetic transition, which is shown in the inset to Fig. 3 starts increasing with Mn concentration for $x \approx 2/3$. This indicates a crossover between the second-order and first-order nature of the transition.

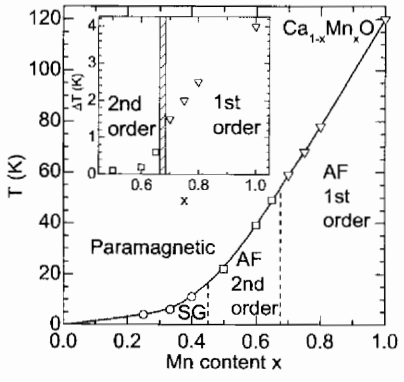

Fig. 3. Magnetic phase diagram of $Ca_{1-x}Mn_xO$. SG denotes spin glass behavior. Two antiferromagnetic phases to which the transition is of first or second order are denoted as "AF 1st order" and "AF 2nd order," respectively. The solid line is a guide to the eye. The inset shows the width of the thermal hysteresis in the ac susceptibility at the AF transition.

The high-temperature ac susceptibility of $Ca_{1-x}Mn_xO$ generally shows Curie-Weiss behavior. Within the framework of the diluted Heisenberg antiferromagnet theory [22], the high-temperature ac mass susceptibility can be described by the formula

$$\chi = \frac{C_M(x)}{\mu(x)(T - \Theta(x))}, \tag{1}$$

where χ is the ac susceptibility after subtraction of the diamagnetic contribution of the host material CaO (equal to $-0.27 \cdot 10^{-6}$ emu/g) and $C_M(x)$ is the molar Curie constant defined as

$$C_M(x) = x\frac{N(g\mu_B)^2 S(S+1)\mu(x)}{3k_B\rho(x)} \tag{2}$$

N is the number of cations per unit volume, S is the effective spin of Mn^{2+} ion, $g = 2$ is the gyromagnetic factor, $\mu(x)$ is the molar mass, $\rho(x)$ is the mass density, $\Theta(x) = \Theta_0 \cdot x$ is the Curie-Weiss temperature

$$\Theta_0(x) = -\frac{2}{3}x\,S(S+1)\sum_P J_P z_P / k_B \equiv \Theta_0 x, \tag{3}$$

where J_P is the exchange integral for a pair of Pth Mn neighbors and z_P is the number of neighbors of Pth order. In the diluted magnetic regime the dominating interactions are between the nearest neighbors. Hence, we may limit the expansion in Eq. (3) to the first order. The Θ_0 constant is then related